International Journal of Physics
and Research (IJPR)
ISSN(P): 2250-0030; ISSN(E): 2319-4499
Vol. 6, Issue 1, Feb 2016, 7-20

THE EFFECT OF ETCHING CURRENT ON THE FORMATION OF ANTIREFLECTION POROUS SILICON COATING FABRICATED BY ELECTROCHEMICAL TECHNIQUE FOR SOLAR CELLS

G. M. YOUSSEF

Department of Physics, Faculty of Science, Ain Shams University, Abbasia, Cairo, Egypt

ABSTRACT

The Effect of different etching current densities on the formation of antireflection porous silicon coating used for Solar Cells industry has been investigated. The results show that both the initial surface morphologies and the anodizing etching condition affected on photoluminescence (PL) and the reflectance of the resulting surface. Large number of pores uniformly distributed on overall surface with average pore diameter from 5.80 to 6.20 nm was observed. The vertices of the straight pyramids of the textured Si wafers are etched away during the electrochemical etching and frustums of the pyramids are formed. The pyramid frustums contain nanopores. The PL intensity increases and the PL peak shows a blue shift that could be related to the quantum size effect (QSE) due to the thinning of filaments by the oxidation process. However, for further increase in etching current density, the PL intensity decreases and PL peak shows a red shift. The explanation of this peak shifts of PL emission of porous silicon (PS) samples is given by type of model, is quantum confinement luminescent center (QCLC) model. The energy band gap values were obtained in terms of optical absorption. The values of the optical energy band gaps, which calculated from the reflectance measurements for direct model transition has a good agreement with the values, which calculated from the PL spectrum. These results confirm that PS has a quasidirect band gap. The PS layers formation on the textured surface presents a significant decrease in the effective reflectance. The surface chemical state of porous silicon was investigated by using IR which is a powerful and an easy-to-use technique. The basic features begin from the knowledge of the bonding to hydrogen, Si-H, and the bonding to oxygen, Si-O.

KEYWORDS: Electrochemical Etching, Porous Silicon, SEM, PL, Absorbance, FTIR, Energy Band Gap, Antireflection Coatings, solar Cell

Received: Nov 30, 2015; **Accepted:** Dec 11, 2015; **Published:** Dec 26, 2015; **Paper Id.:** IJPRFEB20162

Original Article

INTRODUCTION

Uhlir and Turner first reported in the late 1950s that a silicon surface can be covered with a brown film during anodization in HF solutions and suggested that the film was a sub fluoride (SiF_2) grown on the surface during the anodic dissolution [1]. The demonstration in 1990 that porous silicon (PS) could emit efficient tunable visible photoluminescence (PL) at room temperature and attributed to quantum-size effects in crystalline silicon, it was reported by Canham [2]. According to Canham, porous silicon has potential application in optoelectronic and sensor . Generally, there are two methods used to produce porous silicon namely electrochemical etching and chemical etching in the HF based solution [3].

Principal parameters controlling PS mesoporous formation depend on properties of silicon substrate (crystal orientation - doping), etching solution and temperature [4]. The physical properties of porous silicon are

fundamentally determined by the shape and diameter of pores, the thickness and the relative content of Si, voids, and in some cases, the relative content of different Si compounds in the formed porous layer. These parameters depend on preparation conditions, so that it is possible to design materials with physical properties of those between Si and air (or the medium, which fills the pores [5].

The first report of room temperature visible photoluminescence (PL) from porous silicon (PS) structures has attracted wide interest in the scientific community. The mechanism of light emission in porous silicon is not fully understood. One popular hypothesis is that luminescence is due to quantum confinement of charge carriers in narrow crystalline silicon walls separating the pores. The increase in the band gap of PS is possible by reducing the size of the nanocrystallites. Another hypothesis asserts the existence of luminescent surface species trapped on the inner pore walls as the source of light emission. Another concludes that the origin of luminescence can be traced to the presence of surface-confined molecular emitters, such as siloxene (Si6O3H6) derivative, present in porous silicon [6].

The increase in the energy band gap of the PS layer compared with the bulk Si is explained by the observed visible luminescence of the PS layer due to its large internal surface [7]. Thus, photoluminescence (PL) is the best method to determine the energy band gap of the PS layer [8]. In the following, we report on our systematic investigation of the relationship linking PS total porosity, morphology, PL properties and fabrication conditions [4].

The effects of the pore morphology on the optical properties are not well understood. Extensive experimental studies indicate that the observed optical properties depend not only on the porosity but also on the way the PS sample is prepared [9]. The change in pores diameters and change in pores walls dimension have become very important for intensive investigation. In the present study, electrochemical etching with different etching current density was used to fabricate the PS layers [7].

The optical properties of a porous silicon layer are determined by the thickness, porosity, refractive index, and the shape and size of pores and are obtained from both experimental - and model- based approaches. Porous silicon materials are described as a mixture of air, silicon, and, in some cases, silicon dioxide. Porous silicon is a very attractive material for refractive index fabrication because of the ease in changing its refractive index. Structures [10].

A silicon surface is stabilized with hydrogen termination with the hydrofluoric acid (HF) treatment or during the porosification in solution containing fluoride. The surface states, SiHx, influence the properties. The passivated surface undergoes oxidation on putting it in an environment, where some oxidants are present; the oxidation rate depends upon the type of oxidant or the oxidizing ability. Understanding of these chemical states of the silicon surface is indispensable for the study on porous silicon. There are many analytical methods to access the chemical information. Among them, infrared spectroscopy (IR) is a powerful tool to analyze the atomic bonding in a molecule and is widely used [7].

Experimental Measurement

Porous silicon consists of nanometer and micrometer-sized pores. The nanoporous layer has attracted considerable attention due to its visible light emissions [11].

Electrochemical etching of textured crystalline n^+ p silicon wafer were done in electrolytes including hydrofluoric acid (HF) and surfactants (mainly ethanol) forms the porous silicon structure. Ethanol (C_2H_5OH) is often added to facilitate evacuation of H_2 bubbles; these bubbles can easily leave the surface because of the decreased surface tension of the liquid. Additionally, the bubbling enhances the liquid circulation in the electrolyzation cell, which helps the transport of reactants

and side products. To be able to synthesize uniform layers with high reproducibility, the applied anodic current density and etching time are monitored, controlled and kept at a particular constant level required during the process [5].

The Teflon electrochemical cell was made from two-electrode system was connected to the silicon wafer as anode and platinum as cathode. This design allows using the cell for electrochemical etching. Etching only one side of the silicon substrates has been considered in this design, while the backside is completely separated from the etching acid, thereby, the metallization of the backside, which is coated by aluminum, will be protected [12]. The textured crystalline n^+ p silicon wafer samples used in this study were using (100) oriented P-type CZ wafers with resistivity 3-5 Ω cm with a thickness of 450 µm [11]. Before electrochemical etching of silicon, samples substrates were rinsed in de-ionized water and dried in the presence of nitrogen gas after heating in trichloroethylene (isopropyl) for 5 minutes [13]. The PS layers on textured samples were prepared by electrochemical etching in electrolyte composed of HF(40 %): C_2H_5OH (95 %) with a concentrations ratio 1:2 (by their volumes) at etching current densities 15, 25, 35 and 45 mA/cm^2 under constant etching time 20 min which remarket by PS1,PS2,PS3 and PS4 ,respectively . After etching process, the samples have been cleaned by acetone and then immersed in ethanol to clean off the acetone residue. After wards, the samples were dried under nitrogen gas flow [14, 15]

The photoluminescence (PL) was measured by using a monochromator (Jobin Yvon) with an attached charge coupled device. A beam of 325 nm line from argon laser at 10 mW output power was used for excitation. The PS surface was observed by using Scanning Electron Microscopy (SEM) (Model Quanta 250 FEG). The total optical reflectance of the PS layers were obtained using an Optical Reflectometer (JASCO V-570) which equipped with an integrating sphere in the 200–1100 nm wavelength range. The chemical and physical changes affect the properties of porous silicon-based devices. The infrared (IR) spectroscopy is an effective and easy tool for monitoring and/or characterizing the surface state [7]. The Fourier-transform infrared (FTIR) spectrometer used for the measurement of our PS samples is a Nicolet 6700 FTIR thermo scientific class1.

RESULTS AND DISCUSSIONS

SEM studies were done in order to probe the microstructural_variations in PS formed on textured Si-substrates. The pore on the silicon surface has changed the characteristic of porous silicon [16]. For the textured substrate without any PS formation, the surface morphology consists of randomly sized and spaced pyramids homogeneously distributed on the surface and for the PS formed on textured substrate; the surface morphology does not essentially differ from the textured silicon substrate [17].

The results show that the regular porosity and pore size distribution in different locations. It means that the pore diameter and microstructure are depended on anodization conditions such as the etching current density [18]. Figures 1(a) and 1(b) show that uniform texturization throughout the surfaces was achieved by etching for PS1 and PS2. The morphology of PS2 surface gives a smaller size of the pyramids [17]. The SEM images in Figure (1b) illustrate the treated surface with similar grain geometry due to the isotropic character of HF:C_2H_5OH etching and the optimal conditions of current density and etching time [19].

As the etching current density increase the PS film formed for PS3, is noticed that the pyramids are sharply separated and the regions between the pyramids show deep etching as shown in Figure 1(c). Here, there is no evidence of any fracture or cracks formation unlike in the case of textured silicon substrate for the low current densities (15-35

mA/cm^2) and this indicates lower stress for PS films formed on textured silicon substrates [17]. The vertices of the straight pyramids of the textured Si wafers are etched away during the electrochemical etching and frustums of the pyramids are formed. In case of PS formed for PS4 was shown in Figure 1(d), results changing in porosity and the inability of the silicon nanowires to with stand the stress leads to a pronounced cracking pattern is observed. So it is observed that the surface morphology is affected by current density.

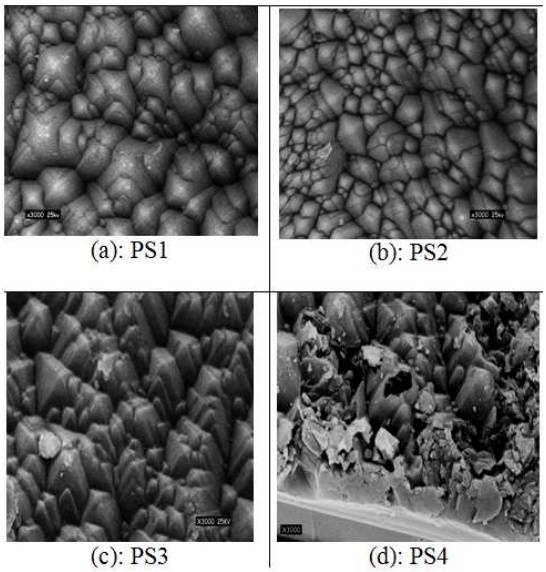

Figure 1: SEM Micrographs Of PS Layers Formed On Textured Crystalline N^+ P Silicon Surfaces after Electrochemical Etching At Different Etching Current Densities: (A) PS1: 15 Ma/Cm^2, (B) PS2: 25ma/Cm^2, (C) PS3: 35ma/Cm^2, (D) PS4: 45ma/Cm^2

The observed dependence of PL spectra from PS on preparation conditions was correlated with PS surface determined by SEM [4]. PL is a process in which a substance absorbs photons and then re-radiates photons. This can be described as an excitation to a higher energy state and then a return to a lower energy state accompanied by the emission of a photon. The PL analysis is useful in the design of the nano scale optical band gap device applications [12].

The prepared porous structure in bulk silicon is strongly responsible for the photoluminescence on its surface, which can be confirmed by shifting in the band gap energy of bulk silicon [20]. Figure 2 shows the room temperature photoluminescence (PL) emission spectra of porous silicon layers grown for different etching current density from 15 mA/cm^2 (PS1) to 45 mA/cm^2 (PS4). The PL was excited using a monochromatic radiation of 325 nm wavelength.

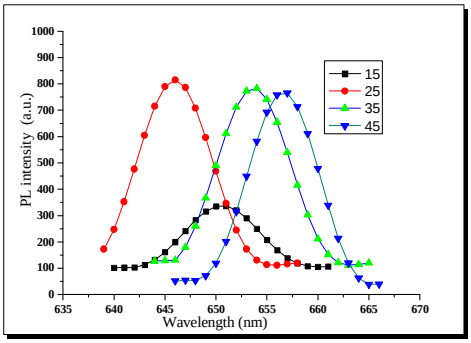

Figure 2: PL Spectra of Different PS Layers Grown Electrochemically for Different Etching Current Densities

As the etching current density is increased from 15 mA/cm^2 of PS1 to 25 mA/cm^2 of PS2, the PL emission peak shows a blue shift. According to the quantum confinement model, PL emission is due to band-to-band transition and is dependent on the size of Si crystallites; smaller crystallites size shifts the emission peak to shorter wavelengths [14, 15]. Hence, the observed increase in PL intensity and blue shifting of the PL could be related to the quantum size effect (QSE) due to the thinning of filaments by the oxidation process [5] and the passivation by a thin silicon oxide film formed at the PSL surface. The PL now appeared shifted towards the blue [21**].** However, when the etching current density is increased from 25 mA/cm^2 of PS2 to 45 mA/cm^2 of PS4 the PL peak shows a red shift. The explanation of this peak shifts of PL emission of PS samples is given by type of model, is quantum confinement luminescent center (QCLC) model. According to QCLC model, the radiative recombination takes place with the help of different luminescent centers of silicon oxide grown on the front surfaces of PS layers. The radiative recombination process leads to the red PL emission. The spectral behavior depends upon the shape and size distribution of Si crystallites [19]. Then, from the PL spectrum, the energy gap was determined by equation [14]:

$$E_g = \frac{hc}{\lambda} \quad (1)$$

where E_g energy gap of the PS, h is Planck constant, **c** is the speed of light and **λ** is the peak wavelength of the photoluminescence [3]. The energy band gap was found to increase from 1.90 and 1.92 eV for the PS layer fabricated for PS1 and PS2, respectively, as seen in Table.1

Table 1: The Average Pore Diameter and the Energy Band Gap (From PL Measurements) of PS Layers Grown Electrochemically For Different Etching Current Densities

Sample	Band Gap Energy (eV)	Average Pore Diameter (d) nm
PS1	1.90	5.88
PS2	1.92	5.80
PS3	1.89	5.91
PS4	1.82	6.20

As current density increases from 25 to 45 mA/cm^2, the samples grown shows distinct color over etched surface. It was noted that PL spectra of structure of PS2, PS3 and PS4 in Figure 1, corresponds to them decrease in the energy gap, respectively, 1.92, 1.89 and 1.82 eV and which are summarized in Table 1.

An estimate of the size of the Si nanocrystallites was determined using effective mass theory [23]. The average pore diameter (d) was calculated by the following equation (2) and summarized in Table 1 for all the PS samples along the different etching current densities.

$$E(eV) = E_g + \frac{h^2}{8d^2}\left[\frac{1}{m_e^*} + \frac{1}{m_h^*}\right] \quad (2)$$

where E (eV) is the energy band gap of PS calculated from the PL peak position, E_g= 1.12 eV is the energy band gap of bulk Si, h is Planck's constant = 4.13 x 10^{-15} eV and m_e^*, m_h^* are the electron and hole effective mass, respectively (at 300 K, m_e^*= 0.19m_o, m_h^* =0.16m_o and m_o=9.109 x10^{-31} Kg).

The resultant values of (d) are calculated and abbreviated in table (1). It is remarkable that as the current density increases the diameter of pores is changed as shown in table 1. This results the alteration in silicon crystallites size hence, photoluminescence wavelength is shifted. According to the variation in the anodization parameters, the shifting of blue or red emission can be observed in Figure 2 [23]. These results are useful for the design of potential applications of nanoscale

PS based materials for the light emitting devices, photovoltaic solar cells, optical filters, photonic devices like distributed Bragg reflectors, microcavity, rugate filters, chemical and bio-sensors [15].

In contrast, PS surface formed on the texturing surfaces had bigger pores. This might be attributed to an increase in surface roughness. The high degrees of roughness of the PS surface implies the possibility of using porous layer as an ARC, because the surface texture reduces the light reflection and increase the light-trapping upon wide wavelength range. This is an important parameter to enhance the photo conversion process for some devices as in solar cells. To confirm that PS can be utilized as anti-refection coating, the reflection measurement was done by using optical reflectometry [24-25].

Figure 3 shows the reflection spectra by using optical reflectometer equipping by integrating sphere of textured surfaces after PS formation, in the wavelength region of 200- 1100 nm. After the electrochemical processing, porous film was presented on the textured surface of the samples, which results in a dramatic decrease in the effective reflectance. It is noted that the reflective behaviors of the resulting surface depend on the initial surface morphologies [14-15].

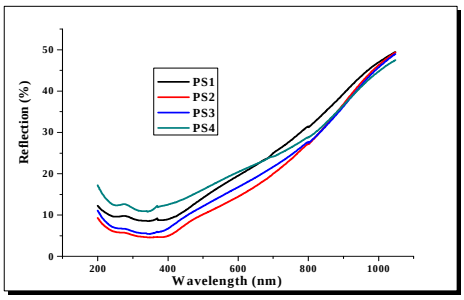

Figure 3: Reflection Spectra of the PS Samples Based on Textured Crystalline N^+ P Silicon Wafers Using Different Etching Current Densities

The reflectance of PS layers formation in the short wavelength range was reduced from 11.19 to 4.59 % at 350 nm. The lowest effective reflectance (4.59 %) was recorded from the PS layer of PS2, which clearly reduced the light reflection and increased the light-trapping at wavelengths ranging from 200 to 500 nm, and a slight increase in the reflection occurred from 500 to 1000 nm, perhaps because of the random distribution of the pores and the decrease or the increasing roughness on the PS surface [26**].** The effective reflectance is increase from 5.66 to 11.19 % as the etching current is increased for samples PS3 and PS4, which was depend on the PS surface formed on the texturing side had bigger pores.

This is clear from the remarkable change in the morphological properties of the treated PS layers Figure 1 [27]. The PS layer consists of nanosilicon crystals and nanopores. Therefore, the refractive index decreased and was controlled by the pores, which led to a decrease in reflection. This believed that the etching current density of PS2 is the optimal value of the electric charges passing through the electrolyte during the anodization process [26].

The low degrees of roughness of the PS surface implies the possibility of using porous layer as an ARC, because the surface texture reduces the light reflection and decrease the light-trapping upon wide wavelength range. This demonstrates that PS could be used as an ARC layer in solar cells for enhancing the photoconversion process and increasing light absorption in the VIS region of the solar spectrum, which is also expected to increase the efficiency of solar cells

The results of the diffused reflectance measurements, shown in Figure 4, are very important for usage in determination the absorption coefficient which can be calculated by using the following Eq: [27]

$$\alpha = \frac{1}{2t} \mathrm{Ln} \frac{(R_{max} - R_{min})}{(R - R_{min})} \quad (3)$$

where t is the film (sample) thickness, R_{max} and R_{min} are the maximum and minimum reflectance in the diffused reflection spectra and R is the reflectance for any intermediate energy photons recorded by the optical spectrophotometer.

The band gap of a material can be determined from a measurement of the absorption coefficient vs. wavelength. According to Tauc relation, the absorption coefficient for energy band gap material is [28-29].

$$\alpha = A [(h\upsilon - E_g)^m] / h\upsilon. \quad (4)$$

where A is the edge width parameter representing the film quality, Eg is the optical energy gap and the parameter m is expressed the type of transition, for direct transition m=1/2 and for indirect transition m=2. When $(\alpha h\upsilon)^{1/m}$ =zero for certain υ_0, then Eg =$h\upsilon_0$. The usual method for determine of the value of Eg involves a plottin1g of $(\alpha h\upsilon)^{1/m}$ versus hυ. The value of the energy gap Eg is determined from the intercept of extrapolation to zero absorption with the photon energy axis. Figure 4 shows the plot $(\alpha h\upsilon)^{1/2}$ versus Eg (hυ), which is used to calculate the energy band gap, considering an indirect allowed transition of PS for samples with different porosity [30]. It is easy to observe that the energy band gap increases from 1.70 to 1.85 eV for the samples PS1 and PS2 (blue shift), subsequently decreases from 1.56 to 1.49 eV for PS3 and PS4 (red shift) respectively. Nevertheless when direct allowed transition for PS is taken into account, for plot a $(\alpha h\upsilon)^2$ versus Eg (hυ), another increase in the energy band gap values from 1.92 to 2.10 eV for the samples PS1 and PS2 (blue shift), subsequently decreases from 1.97 to 1.85 eV for PS3 and PS4 (red shift) respectively, which are summarized in Table 2.

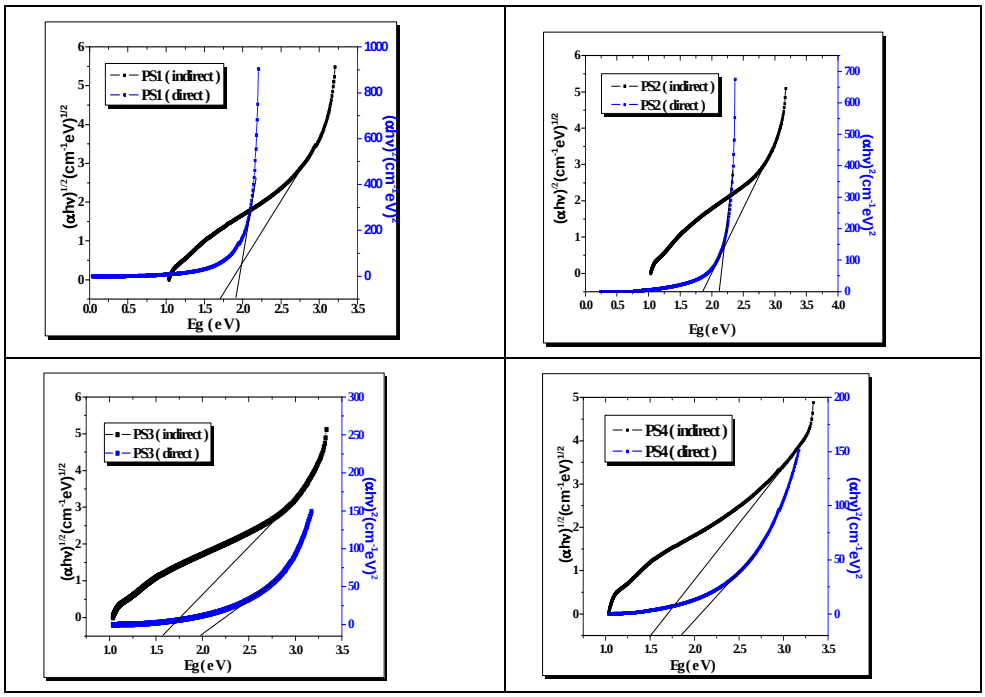

Figure 4: The Optical Energy Band Gap Using Direct and Indirect Transition Models (Reflection Spectra Measurements) of the PS Samples Based on Textured Crystalline N^+ P Silicon Wafers Using Different Etching Current Densities

Table 2: The Optical Energy Band Gap Using Direct and Indirect Transition Models (Reflection Spectra Measurements) of the PS Samples Based on Textured Crystalline N^+ P Silicon Wafer Using Different Etching Current Densities

Sample	Band Energy Gap(eV) From Indirect Model Transition	Band Energy Gap(eV) from Direct Model Transition
PS1	1.70	1.92
PS2	1.85	2.10
PS3	1.56	1.97
PS4	1.49	1.85

The obvious blue shift in absorption band edge in the case of direct or indirect allowed transition has been due to increasing porosity and decreasing size in Si (so-called quantum size effect). As for the red shift in absorption band has been due to decreasing in porosity and increasing size in Si. The values of the optical energy band gaps, which calculated from direct model transition, has a good agreement with the values, which calculated from the PL spectrum (Table 1). These results confirm that PS has a quasidirect band gap [30]. This is an important parameter to enhance the photoconversion process for some devices as in solar cells [31]. The character of the PS with a variable index can explain the experimental results. As mentioned above, the effective refractive index of PS is an intermediate value between air and silicon and can be variable by the change of porosity, thus, different PS morphologies result in different values of refractive index [32].

The refractive index n is an important physical parameter related to microscopic atomic interactions. The crystalline structure represented by a delocalized picture, n will be closely related to the energy band structure of the material, complicated quantum mechanical analysis requirements and the obtained results.

Many attempts have been made to relate the refractive index and the energy gap Eg through simple relationships. However, these relationships of n are independent of temperature and incident photon energy. Here, The various relationships between n and Eg will be reviewed. Ravindra et al. [33] suggested different relationships between the band gap and the high frequency refractive index and presented a linear form of n as a function of Eg:

$$n = \alpha + \beta E_g \quad (5)$$

where $\alpha = 4.048$ and $\beta = -0.62\ eV^{-1}$.

To be inspired by simple physics of light refraction and dispersion, Herve and Vandamme [34] proposed an empirical relation

$$n = \sqrt{1 + \left(\frac{A}{E_g + B}\right)^2} \quad (6)$$

where A = 13.6 eV and B = 3.4 eV.

Ghosh et al. [35] took a different approach to the problem by considering the band structural and quantum-dielectric formulations of Penn [36] and Van Vechten [37]. Introducing A as the contribution from the valence electrons and B as a constant additive to the lowest band gap Eg, the expression for the high-frequency refractive index are written as

$$n^2 - 1 = \frac{A}{(E_g + B)^2} \quad (7)$$

where A = $25E_g$ + 212, B = $0.21E_g$ + 4.25 and (Eg + B) refers to an appropriate average energy gap of the material. Thus, these three models of variation n with energy gap have been calculated. The calculated refractive indices of the end-point compounds are calculated in Table 3. These results are verified by calculating the optical dielectric constant ε_∞, which is dependent on n; hence, $\boldsymbol{\varepsilon_\infty = n^2}$. In Table 3, the calculated values of $\boldsymbol{\varepsilon_\infty}$ using the three models are investigated. As with Ghosh et al. [35], this is more appropriate for studying solar cell optical properties.

Table 3: Calculated Refractive Indices for PS Using Ravindra Et Al. [33], Herve and Vandamme [34] and Ghosh Et Al.[35] Models Compared with Others Corresponding to Optical Dielectric Constant. (A Ref. [33], B Ref. [34] in Addition, C Ref. [35])

Sample	E_g (eV)	n	$\boldsymbol{\varepsilon_\infty}$
PS1	1.92	2.88[a], 2.74[b], 2.64 [c]	8.32 [a], 7.53 [b], 7.02 [c]
PS2	2.10	2.77 [a], 2.66 [b], 2.59[c]	7.67 [a], 7.11[b], 6.72 [c]
PS3	1.97	2.85 [a], 2.72 [b], 2.43[c]	8.14 [a], 7.41[b], 5.94 [c]
PS4	1.85	2.93 [a], 2.77 [b], 2.67[c]	8.59 [a], 7.71[b], 7.13 [c]

These results are verified by calculating the optical dielectric constant ε_∞, which is dependent on n; hence, $\boldsymbol{\varepsilon_\infty = n^2}$. In Table 3, the calculated values of $\boldsymbol{\varepsilon_\infty}$ using the three models are investigated. As with Ghosh et al. [35], this is more appropriate for studying solar cell optical properties. Therefore, high absorption may be attributed to an increase in sensor efficiency [38]. The attenuation of the reflectivity is due to scattering and transmission at the porous and bulk interfaces.

This parameter has its significant role in order to enhance the light conversion efficiency of solar cells. The PS layer consists of nanosilicon crystals and nanopores Therefore; the decreasing in refractive index was controlled by the pore size, which led to a decrease in reflection. A change in the surface passivation, as well as dielectric effects, can produce wavelength shifts [26].

The surface of electrochemically etched porous silicon was passivated with hydrogen just after preparation. The surface is gradually oxidized under ambient atmosphere, and the rate depends upon the ambient condition. The chemical and physical changes affect the properties of porous silicon-based devices. Proper understanding of the surface is important, and infrared (IR) spectroscopy is an effective and easy tool for monitoring and/or characterizing the surface state. Silicon is almost transparent to IR light, and hence the convenient transmission measurement is applicable to films and membranes of porous silicon. The measurement technique is first described, and then assignments of absorption bands in the spectra are given for the hydrogen-terminated and oxidized surface. The prevention of oxidation and the functionalization of porous silicon surface are important for many practical uses, where IR measurements can be used to monitor the surface [39].

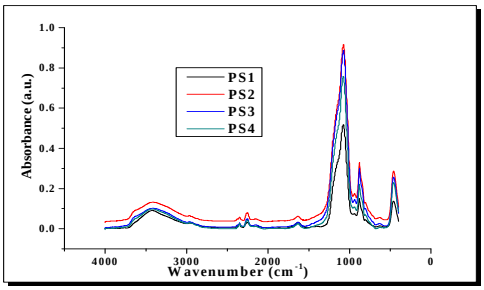

Figure 5: Figure 4 Shows the FTIR Spectra of the PS Samples Based on Textured Crystalline N^+ P Silicon Wafer Using Different Etching Current Densities

Silicon is tetravalent, and the crystal has a tetrahedral structure. Hydrogen molecules can bond with silicon in the crystal as $SiH_{x,}$ (x =1–3). The peak assignment had been performed comparing with the spectra of the related materials, amorphous hydrogenated silicon (a-Si:H) and HF-treated silicon [40-42]. Porous silicon and a-Si:H resemble with each other except the crystallinity. Their FTIR spectra are similar. HF-treated silicon is of course monocrystalline and measured by the reflection method. The spectrum is exactly that of porous silicon. Pores in microporous silicon are randomly oriented, and the polarized beam gives similar spectra. The assignment of the absorption bands appearing in porous silicon is investigated experimentally [43].

Silicon is a very less noble element, and it is prone to be oxidized under ambient atmosphere. The oxidation can be easily followed by FTIR with the absorption mode. The absorption bands appear in the same frequencies as the transmission spectroscopy, but the intensity is different because of the difference in the optical path. [44-45]. The passivating capability of PS was studied using Fourier transform infrared spectroscopy (FTIR) the appearance of bonds related to Si–H_x, and Si–O–Si species [46].

In the FTIR spectra Figure 5 of the PS the peak at 452 cm^{-1} is attributed to a bending vibration of Si-O-Si bonds, which are dependent on the oxidation degree of porous silicon and the peaks at 891 cm^{-1} were assigned to a wagging vibration of Si-H_2 bonds [16]. A large vibration absorption band is observed at 1063 cm^{-1}, corresponding to a pure Si-O stretching in Si–O–Si mode. The peak at 1625 cm^{-1}, is assigned to C=O carbon oxygen bond. Moreover, the spectrum also shows the presence of a vibration band at 2246 cm^{-1} indicating the presence of SiH_3 stretching bonds. A vibration OH Stretching water vapor band at the peak at 3421 cm^{-1}[47].

Table 4: Wavenumber Position and Attribution of the Absorption Peaks Observed in PS Samples Using Different Etching Current Densities

Absorption Band (cm-1)	Mode	Attribution
452	Si-0-Si	Bending
891	Si-H_2	Wagging
1063	Si-O	Stretching in O-Si-O
1625	C=O	Carbon oxygen bond
2246	SiH_3	Stretching
3421	OH	Stretching water vapor

A broad band in the 1300–1500 cm^{-1} region is sometimes found in some spectra. This produced by post-oxidation during the sample drying procedure [43]**.** Chemical bonds and their IR resonance positions (the vibration modes) detected in PS are shown in Table 4. These peak positions are compared with others reported work and have found good matching. For the application of solar cells, top layer is required to be low reflective surface.

CONCLUSIONS

Our investigations show that both the initial surface morphologies and the anodizing etching condition affected on PL and the reflectance of the resulting surface. Large number of pores were uniformly distributed on overall surface with average pore diameter from 5.80 to 6.20 nm. The PL intensity increases and the PL peak shows a blue shift could be related to the quantum size effect (QSE) due to the thinning of filaments by the oxidation process. However, for further increase in etching current density, the PL intensity decreases and PL peak shows a red shift. The band gap values were obtained in terms of optical absorption. The values of the optical energy band gaps, which calculated from the reflectance measurements for direct model transition has a good agreement with the values, which calculated from the PL spectrum.

These results confirm that PS has a quasidirect band gap. Also, the experimental values of refractive indices and dielectric constants of the samples were calculated based on different relationships by utilizing band gap values to investigate the optical properties of PS layers. The PS layers formation on the textured surface presents a significant decrease in the effective reflectance. From the obtained results, we can conclude that PS can be used as antireflection coatings and passivation layers for the application of solar cells.

REFERENCES

1. *X. G. Zhang, (2004) Morphology and Formation Mechanisms of Porous Silicon, Journal of the Electrochemical Society 151:69-80, doi:10.1149/1.1632477.*
2. *B Gelloz, (2014) Photoluminescence of Porous Silicon, Handbook of Porous Silicon, Springer, DOI 10.1007/978-3-31905744-6-32.*
3. *Dwight Tham Jern Ee, Chan Kok Sheng and M.I.N. Isa, (2011) Photoluminesc- scence of porous silicon prepared by chemical etching method, The Malaysian Journal of Analytical Sciences 15: 227- 231.*
4. *J. Dian, A. Macek, (2004) SEM and HRTEM study of porous silicon relationship between fabrication, morphology and optical properties, Applied Surface Science 169–174.*
5. *D. K. Salucha, A. J. Marcinkevicius, (2007) Investigation of Porous Silicon Layers as Passivation Coatings for High Voltage Silicon Devices, Electronic and Electrical Engineering 7: 79.*
6. *Kasra Behzad, Wan Mahmood Mat Yunus, (2012) Effect of Etching Time on Optical and Thermal Properties of P-Type Porous Silicon Prepared by Electrical Anodization Method, Advances in Optical Technologies, I D 581743, doi: 10.1155/2012/581743.*
7. *Yukio H. Ogata , (2014) Characterization of Porous Silicon by Infrared Spectro- scopy, Handbook of Porous Silicon: 473-480, DOI 10.1007/978-3-319-05744-6-48.*
8. *Khaldun A. Salman, Khalid Omar, Z. Hassan, (2011) The effect of etching time of porous silicon on solar cell performance, Superlattices and Microstructures 50: 647–658.*
9. *L. Canham (ed.), (2014) Handbook of Porous Silicon, Springer International Publishing Switzerland, DOI 10.1007/978-3-319-05744-6-1*
10. *Honglae Sohn , (2014) Refractive Index of Porous Silicon. Handbook of Porous Silicon: 231-243, DOI 10.1007/978-3-319-05744-6-25.*
11. *Fatima I. Sultan, Amna A. Slman, (2013) I-V and C-V characteristics of porous silicon nanostructures by electrochemical etching, Eng. & Tech. Journal 31, No.3.*
12. *P. N. Patel, V. Mishra, A. K. Panchal, (2012) Synthesis and characterization of nano scale porous silicon photonic crystals for optical device and sensing application, Journal of Optoelectronics and Biomedical Materials 4:19-28.*
13. *Wisam J. Aziz, Khaled Omar, (2009) The performance of silicon solar cell with different texturing processes, Journal of optoelectronics and Advanced Materials 11, No.11: 1632-1636.*
14. *G .M. Youssef, S.Y. EL- Zaiat, M. EL-Malky, H.A. Nawar, (2015) Preparation and physical chactarization of porous silicon layers for sensing application, International Journal of Applied, Physical and Bio-Chemistry Research 5: 33-48. G. M.Youssef, M.M. El-Nahass, S.Y. El-Zaiat, M.A. Farag, (2015) Effect of porosity on the electrical and photoelectrical properties of textured n^+ p silicon solar cells, (2015) Materials Science in Semiconductor Processing 39: 457-466.*

15. *Shailesh N. Sharma, R.K. Sharma et al, (2006) Demonstration of the formation of porous silicon films with superior mechanical properties, morphology and stability, Materials Letters 60: 1166 – 1169.*

16. *Ou Weiying , Zhao Lei, Diao Hongwei, Zhang Jun.Wang Wenjing, (2011) Optical and electrical properties of porous silicon layer formed on the textured surface by electrochemical etching, Journal of Semiconductors 32, No. 5.*

17. *Khalid Omar, Asmiet Ramziy, Khaldun A. Salaman, Z. Hassan, (2011)*

18. *Characterization of Porous Si Solar Cell, Journal of Advanced Science and Engineering Research 1:68-75.*

19. *Asmiet Ramizya, Z. Hassana, Khalid Omara et al., (2011) New ptical features to enhance solar cell performance based on porous silicon surfaces, Applied Surface Science 257:6112–6117.*

20. *R. S. Dubey and D. K. Gautam, (2009) Synthesis and characterization of nanocrystalline porous Silicon layer for solar cells applications, Journal of Optoelectronic and Biomedical Materials.1: 8-14.*

21. *M.A. Vasquez-A, G. Aguila Rodrıguez, et al., (2007) FTIR and photoluminescence studies of porous silicon layers oxidized in controlled water vapor conditions, Revista Mexicana De Fi´sica 53: 431–435.*

22. *Daisy Verma , Firoz Khan, S.N. Singh, P.K. Singh, (2012) Correlation between reflectivity and photoluminescent properties of porous silicon films, Electronic Materials Division.*

23. *R. S. Dubey, D. K. Gautam, (2009) Photoluminscence and surface morphology of nanostructured porous silicon, Chalcogenide Letters: 523-528.*

24. *Asmiet Ramizy, Wisam J. Aziz, Z. Hassan, Khalid Omar, K. Ibrahim, (2011) Improved performance of solar cell based on porous silicon surfaces, Optik 122: 2075-2077.*

25. *Gorecka-Drzazga, (2005) Micro and nano structurization of semiconductor surfaces, Bulletin of Polish Academy of Sciences Technical Sciences 53, No. 4.*

26. *Khaldun A. Salman, Khalid Omar, Z. Hassan, (2011) The effect of etching time of porous silicon on solar cell performance, Superlattices and Microstructures 50: 647-658.*

27. *Dubey, R. S, Gautam, D.K, (2011) Synthesis and characterization of porous silicon layers, Optik 122: 494-497.*

28. *Mortezaali, S. Ramezani Sani, F. Javani Jooni, (2009) Correlation between poristy of porous silicon and optoelectronic properties, Journal of Non-Oxide Glasses 1, No. 3: 293-299.*

29. *N. F. Mott, E. A. Davis, (1979) Electronic process in non-crystalline materials, Calendron press, Oxford.*

30. *Q. Humayun, M. Kashif, and U. Hashim, (2013) Structural, Optical, Electrical, and Photoresponse Properties of Postannealed Sn-Doped ZnO Nanorods, Journal of Nanomaterials, ID 792930.*

31. *Khalid Omar, Y. Al-Douri, Asmiet Ramizy, Z. Hassan, (2011) Stiffness properties of porous silicon nanowires fabricated by electrochemical and laser induced etching, Superlattices and Microstructures 50:119-127.*

32. *Ibraheem Mousa Mohammed1, Alaa Hussein Shnieshil, (2013) Characteristics Study of Porous Silicon Produced by Electrochemical Etching technique, International Journal of Application or Innovation in Engineering & Management.*

33. *N.M. Ravindra, S. Auluck, V.K. Srivastava, (1979) On the Penn gap in semico-nductors, Phys. Stat. Sol. (b) 93 K155.*

34. *P.J.L. Herve, L.K.J. Vandamme, (1995) Empirical temperature dependence of the refractive index of semiconductors, J. Appl. Phys. 77: 5476.*

35. *D.K. Ghosh, L.K. Samanta, G.C. Bhar, (1984) A simple model for evaluation of refractive indices of some binary and ternary*

mixes crystals, Infrared Phys 24: 34.

36. *R. Penn, (1962) Wave-number-dependent dielectric function of semiconductors, Phys. Rev 128: 2093.*
37. *[37] J.A. Van Vechten, (1969) Quantum dielectric theory of electronegativity in*
38. *covalent systems I. Electronic dielectric constant, Phys. Rev 182: 891.*
39. *G.A. Samara, (1983) Temperature and pressure dependences of the dielectric constants of semiconductors, Phys. Rev. B 27: 3494.*
40. *Ogata Y, Niki H, Sakka T et al, (1995) Oxidation of porous silicon under water-vapor environment Electrochemical Soc 142: 1595-1601.*
41. *Lucovsky G, Nemanich R, Knights J, (1979) Structural interpretation of the vibrational-spectra of a-Si:H alloys. Phys Rev B 19: 2064–2073.*
42. *Knights J, Lucovsky G, Nemanich R, (1978) Hydrogen-bonding in silicon-hydrogen alloys. Phil Mag B 37: 467-475.*
43. *Burrows V, Chabal Y, Higashi G et al, (1988) Infrared- spectroscopy of Si (111) surfaces after HF treatment – hydrogen termination and surface-morphology Appl Phys Lett 53: 998–1000*
44. *Ogata Y, Niki H, Sakka T et al, (1995) Hydrogen in porous silicon - vibrational analysis of SiHx species. J Electrochemical Soc 142: 195–201.*
45. *Gupta P, Dillon A, Bracker A et al, (1991) FTIR studies of H_2O and D_2O decomposition on porous silicon surfaces. Surf. Sci. 245: 360-372.*
46. *Borghesi A, Guizzetti G, Sassella A et al, (1994) Induction-model analysis of Si- H stretching mode in porous silicon. Solid State Commun 89: 615–618.*
47. *Ben Rabha Mohamed, Hajjaji Anouar, Bessais Brahim, (2012) Improvement of multicrystalline silicon solar cell performance via chemical vapor etching method-based porous silicon nanostructures, Solar Energy 86: 1411–1415.*
48. *Binay K. Dutta, Tayseir M. Abd Ellateif, and Saikat Maitra, (2011) Development of a Porous Silica Film by Sol-gel Process, World Academy of Science, Engineering and Technology 5: 1-27.*